1987ApJ...319..601U

THE ASTROPHYSICAL JOURNAL, 319:601–613, 1987 August 15
© 1987. The American Astronomical Society. All rights reserved. Printed in U.S.A.

# FORMATION OF STELLAR SHELLS AND X-RAY CORONAE AROUND ELLIPTICAL GALAXIES

MASAYUKI UMEMURA
Department of Physics, Hokkaido University and Tokyo Astronomical Observatory, University of Tokyo
AND
SATORU IKEUCHI
Tokyo Astronomical Observatory, University of Tokyo
*Received 1986 October 23; accepted 1987 February 9*

## ABSTRACT

We propose a wind-accretion flow interaction model for the formation of extended multiple stellar shells and hot X-ray coronae around elliptical galaxies. We examine the successive interactions of a hot galactic wind with nonstationary ambient gas, which accretes onto the galaxy. The similarity solution for the interaction of a wind with accreting gas is obtained, and we perform the numerical simulations of the successive collisions between a wind and an accretion flow. The dark matter, the time variations of wind luminosities, and the explosive energy release from young stellar components of shells are taken into account. It is shown that multiple stellar shells actually can be produced by such successive collisions. If the galaxy possesses a dark halo with a mass nearly 10 times that of the baryonic component, the ejected hot gas confined in the envelope of the galaxy yields X-ray coronae with luminosities as high as those observed.

If the wind luminosity is below a critical luminosity $L_{w,\mathrm{crit}}$, the ram pressure of accreting gas suppresses the outflow of the wind, so that there will be no extended stellar shells formed by this mechanism. We obtained $L_{w,\mathrm{crit}}$ analytically and numerically. $L_{w,\mathrm{crit}}$ becomes larger if the ambient gas density is higher. This may be one of the reasons why shell galaxies are preferentially found in the regions of low galaxy density, since the ambient gas density is lower in such regions than in clusters. In the present scenario, there is a tendency for the younger shells to be located in the outer regions around a shell galaxy. This can be tested by the observations of color indices of shells over a wide range of distances.

*Subject headings:* galaxies: internal motions — galaxies: structure — galaxies: X-ray — hydrodynamics

## I. INTRODUCTION

Within the last several years, we have encountered two conspicuous discoveries regarding elliptical galaxies. One is that of the extended concentric faint multiple shells in the outer envelopes of numerous elliptical galaxies (Malin and Carter 1980, 1983; Schweizer and Ford 1985; Athanassoula and Bosma 1985). The other is that of the X-ray emitting gaseous coronae surrounding early-type galaxies (Forman *et al.* 1979; Forman, Jones, and Tucker 1985; Canizares, Fabbiano, and Trinchieri 1987).

A significant statistical property on shell galaxies is the clear tendency that shell galaxies are preferentially found in the regions of low galaxy density. Nearly half of all shell galaxies are classified as isolated, and only several percent of shell galaxies belong to rich groups or clusters of galaxies (Malin and Carter 1983; Schweizer and Ford 1985). At present, the constituents of shells are considered to be stars, and photometry of shells has shown that shells are composed of stellar populations not older than the underlying galaxies, often similar to the disk population (Carter, Allen, and Malin 1982; Fort *et al.* 1986; Pence 1986). The number of shells detected per an elliptical galaxy ranges from 1 to $\sim 20$. In general, shells exhibit incomplete circles, and they are distributed in a very wide range of distances, as fas as $\sim 200\ (H_0/50\ \mathrm{km\ s^{-1}\ Mpc^{-1}})^{-1}$ kpc (Malin and Carter 1983).

Several theories of shell formation have been proposed so far. Schweizer (1980) suggested that shells or ripples could be the result of mergers, and this suggestion motivated $N$-body simulations by Quinn (1982, 1984) on the accretion of a companion galaxy into a rigid potential well. These simulations have been extensively developed by Huang and Stewart (1985), Dupraz and Combes (1986), and Hernquist and Quinn (1987). Hernquist and Quinn (1987) found that sharp-edged features are a general property of interactions between low velocity dispersion systems and massive galaxies. In particular, it is possible to form shells by mass transfer in parabolic and bound nonradial encounters, although the exceptionally well regulated shells as seen around NGC 1344 and NGC 3923 are probably formed as a result of collisions from nearly radial companion orbits. On the other hand, Fabian, Nulsen, and Stewart (1980) and MacDonald and Bailey (1981) suggested that a stellar shell could form in a shocked galactic wind region. However, if it has been formed recently by a hot galactic wind, its color would be even bluer than observed, as Carter, Allen, and Malin (1982) remarked. Williams and Christiansen (1985) proposed a more elaborated galactic wind model based on the idea that shells are composed of stars formed in an expanding blast wave, which is driven by a galactic wind due to the nuclear activity in the early history of the galaxy. In this model, multiple shells may be caused by repeated episodes of shell cooling and heating by supernovae on the shells.

On the other hand, X-ray emitting gaseous coronae have been detected with the *Einstein Observatory* around a large number of early-type galaxies. Forman, Jones, and Tucker (1985) and Canizares, Fabbiano, and Trinchieri (1987) found that the hot gaseous coronae associated with bright early-type galaxies are universal. The measured X-ray luminosities are



© American Astronomical Society • Provided by the NASA Astrophysics Data System

1987ApJ...319..601U



$10^{39}$–$10^{42}$ ergs $s^{-1}$ at the 0.5–4.5 keV band. The hot coronae often extend as far as $\sim 100$ kpc, well beyond the Holmberg radius of the galaxy, and hot gas masses amount to $5 \times 10^{8-10}$ $M_\odot$. If the hot coronae were used as probes, the total galaxy masses are inferred to be $\sim(1\text{–}5) \times 10^{12}$ $M_\odot$. These masses imply a large mass-to-luminosity ratio, $\sim 100$ in solar units, which suggests the presence of predominant massive dark halos.

At present, we have some examples which have both shells and X-ray coronae such as NGC 1316, NGC 1395, NGC 3923, and NGC 5128. The fact that shell galaxies are often found to be isolated, and even isolated galaxies have X-ray coronae suggests that these features might be due to an intrinsic physical process of galaxies. In this paper, we tentatively consider a hot galactic wind as an intrinsic physical process which produces both shell structures and X-ray coronae. Supernova-driven galactic winds (Mathews and Baker 1971) have been thought as an important gas removing mechanism from elliptical galaxies which show little evidence for appreciable amounts of interstellar gas (Faber and Gallagher 1976). Fabian, Nulsen, and Stewart (1980) and Williams and Christiansen (1985) related galactic winds to the formation of shells around E galaxies, but we are still left with how a well-regulated multiple shell system is actually formed by galactic winds. We propose a model of sequential stellar shell formation due to *successive* collisions of a galactic wind with *accreting* ambient matter which is left over in the process of the galaxy formation. The outline of the sequential stellar shell formation is as follows: a wind out of the galaxy sweeps up the accreting gas to create a cooled thin shell, which is disrupted by gravitational instability to induce star formation. Subsequently the wind blows through this stellar shell and interacts again with the accreting external gas to generate another dense gaseous shell, which results in the next stellar shell by fragmentation. This sequence continues until the newly formed gaseous shell is not subject to the gravitational instability. In such a manner, concentric multiple stellar shells can be created as a natural consequence of interactions of the wind with accreting matter. Furthermore, the hot winds may produce X-ray emitting coronae, because the temperature of supernova-driven winds is expected to be $\sim 10^7$ K (Mathews and Baker 1971; MacDonald and Bailey 1981; White and Chevalier 1983). In this paper, we adopt a spherically symmetric model, although shells generally exhibit incomplete arcs. With a spherical model we can efficiently simulate a gravitating multicomponent system composed of gaseous matter, a collisionless stellar component, and dark matter. The effect of nonsphericity will be examined elsewhere. In § II, we obtain the similarity solution for the interaction of a galactic wind with accreting ambient matter. In § III, the numerical model for the calculations of successive collisions between a galactic wind and accreting matter is described in detail. The numerical results on the formation of multiple stellar shells and X-ray coronae are given in § IV. In § V, the numerical results are compared with the observational data.

## II. SIMILARITY ANALYSIS

In a wide variety of astrophysical contexts, similarity solutions for the interaction of a stellar wind with ambient matter have been examined by many authors (Dyson and deVries 1972; Avedisova 1972; Weaver *et al.* 1977; Sakashita, Hanami, and Umemura 1984). These works have been focused mainly on the interaction with *stationary* ambient matter, while Dopita (1981) explored the stellar wind confined by ram pressure in a massive collapsing cloud. As for stellar winds, gravity has been often reasonably ignored, but in dynamical processes on a galactic scale the gravity should be inevitably included. Williams and Christiansen (1985) obtained the similarity solution for a gravitating blast wave driven by an energetic galactic wind for the *stationary* interstellar matter.

Here we present the similarity solution for the interaction of a galactic wind with the *accreting* ambient matter in a gravitational field. In a usual scenario of the galaxy formation from density fluctuations in the early universe, the bound material falls to form a galaxy (Gunn and Gott 1972; Umemura and Ikeuchi 1985). In this process, a certain fraction of material is expected to be left over from galaxy formation, and it will accrete onto the galaxy (Gunn 1977). When the wind activity sets in, the wind ejected from the galaxy will interact with this accreting material.

### *a) Expansion Law of a Wind against Accreting Matter*

We suppose a power law as an initial density distribution of accreting ambient gas: $\rho_{g0}(r) = \rho_c(r/r_c)^{-p}$. The wind luminosity $L_w$ is assumed to be constant. The effect of time variations of $L_w$ is numerically investigated later. The equation of motion for a pressure-driven thin shell against accreting gas is described as

$$\frac{d}{dt}(M_s V_s) = 4\pi R_s^2 P - \frac{GM_s}{R_s^2}\left(M_G + \frac{1}{2}M_s\right) + 4\pi R_s^2 \rho_g(R_s)(V_s - v)v , \quad (1)$$

where $P$ is the internal pressure and the subscript $s$ denotes physical quantities associated with the shell. The quantity $M_G$ is the mass of the central galaxy, which is treated as a point mass here. The quantity $v$ is the inward velocity of accreting gas at the time when it just collides with the shell. The last term in equation (1) represents the momentum loss rate due to the accreting gas. This equation should be coupled with the mass conservation equation for the accreting gas and the energy conservation equation for the hot bubble produced by the galactic wind:

$$R_s^2 \rho_g(R_s) dR_s = r_0^2 \rho_{g0}(r_0) dr_0 , \quad (2)$$

$$\frac{d}{dt}\left[\frac{4\pi}{3(\gamma - 1)} R_s^3 P\right] = L_w - 4\pi R_s^2 P V_s , \quad (3)$$

where $r_0$ is the initial radius of the accreting gas which falls on $R_s(t)$ at $t$. The adiabatic exponent $\gamma$ is 5/3. Equations (1), (2), and (3) can be reduced to

$$\frac{d}{dt}\left[R_s^3 \frac{d}{dt}(M_s V_s) + GR_s M_s\left(M_G + \frac{1}{2}M_s\right) - 4\pi r_0^2 \rho_{g0}(r_0)\frac{dr_0}{dR_s}(V_s - v)v\right] = 2L_w R_s . \quad (4)$$

In this equation, we neglect self-gravity, as far as the global motion is concerned. This assumption is justified, if $M_s$ is much smaller than $M_G$. However, we note here that the role of self-gravity cannot be neglected in the argument of the gravitational instability of a thin shell, as shown later.

The infall velocity $v$ can be estimated by means of spherical perturbation theory (Peebles 1982). Supposing an energy perturbation $\delta_i$ is set up at an early epoch in an Einstein–de Sitter

© American Astronomical Society • Provided by the NASA Astrophysics Data System

1987ApJ...319..601U



universe, then

$$\frac{v^2}{2} - \frac{GM}{r} = -\delta_i \frac{GM}{r_i}, \quad (5)$$

where $r_i$ is the unperturbed radius. The radius $r_i$ is determined by relations $(H_i r_i)^2/2 = GM/r_i$ and $H_i = H_0(1 + z_i)^{3/2}$, where $M$ is the mass within $r_i$. The energy perturbation $\delta_i$ is related to the primordial density fluctuation by $\delta_i = 5/3(\delta\rho/\rho)_i$ (Peebles 1982; Ikeuchi and Umemura 1984). From equation (5), we obtain the infall velocity:

$$v = -\left[\frac{2GM}{r}(1 - \Delta)\right]^{1/2}, \quad (6)$$

with

$$\Delta \equiv \delta_i \frac{r}{r_i} = \delta(z)(1 + z)\left(\frac{H_0^2}{2GM}\right)^{1/3} r, \quad (7)$$

where a relation for linear perturbations, $\delta_i/\delta(z) = (1 + z)/(1 + z_i)$, was used. If the formation epoch of elliptical galaxies is inferred to be $z_{GF} \approx 3$ (Wyse 1985), when $\delta(z_{GF}) \approx 1$, we can evaluate $\Delta$ as

$$\Delta \approx 0.6\left(\frac{M}{10^{11}\ M_\odot}\right)^{-1/3}\left(\frac{r}{100\ \text{kpc}}\right), \quad (8)$$

by using $H_0 = 50$ km s$^{-1}$ Mpc$^{-1}$. (This value for $H_0$ is assumed hereafter in this paper.) Thus, if the flow is in the range of $r < 100$ kpc, we can reasonably assume that the infall velocity is equal to the free-fall velocity, $dr/dt = v = -(2GM_G/r)^{1/2}$. By integrating this, we obtain a relation between $r_0$ and $R_s$,

$$r_0^{3/2} = R_s^{3/2} + \tfrac{3}{2}(2GM_G)^{1/2}t. \quad (9)$$

The density enhancement of accreting gas is calculated by equation (2) and a relation led by equation (9), which is

$$\frac{dr_0}{dR_s} = \left(\frac{R_s}{r_0}\right)^{1/2}. \quad (10)$$

As usual, we search for a solution in the form of $R_s(t) = (at)^n$ which satisfies equations (4), (9), and (10). As a result, we find a similarity solution for a special case:

$$p = \tfrac{1}{2}, \quad n = \tfrac{2}{3}. \quad (11)$$

The value $a$ is determined by

$$a^3 + \frac{5}{4}la^2 + \frac{1}{4}l^2a - q\left(\frac{a}{a + l}\right)^{5/3} = 0, \quad (12)$$

where $l = 3(2GM_G)^{1/2}/2$ and $q = 135L_w/224\pi\rho_c r_c^{1/2}$. Equation (12) has two nonzero real solutions if

$$q \geq 2.05l^3. \quad (13)$$

This requirement can be rewritten as

$$L_w \geq L_{w,\,\text{crit}} = 8.7 \times 10^{41}\left(\frac{\rho_c}{10^{-27}\ \text{g cm}^{-3}}\right)\left(\frac{r_c}{10\ \text{kpc}}\right)^{1/2} \times \left(\frac{M_G}{10^{11}\ M_\odot}\right)^{3/2} \text{ergs s}^{-1}; \quad (14)$$

$L_{w,\,\text{crit}}$ is a critical luminosity, above which the wind can blow outward against the ram pressure of accreting gas. This is to be compared with the total luminosity of the wind,

$$L_w = \dot{M}\left[\frac{V_w^2}{2} + \frac{kT_w}{\mu_H(\gamma - 1)}\right];$$

$L_w$ is evaluated by the typical values for wind properties (Mathews and Baker 1971; MacDonald and Bailey 1981; White and Chevalier 1983):

$$L_w = \left(\frac{\dot{M}}{1\ M_\odot\ \text{yr}^{-1}}\right)\left[3.2 \times 10^{41}\left(\frac{V_w}{1000\ \text{km s}^{-1}}\right)^2 + 1.3 \times 10^{41}\left(\frac{T_w}{10^7\ \text{K}}\right)\right] \text{ergs s}^{-1}. \quad (15)$$

For a strong supersonic wind ($V_w \gg c_s$), $L_w$ is equal to the mechanical luminosity ($\dot{M}V_w^2/2$). Since $L_{w,\,\text{crit}}$ becomes greater with increasing $\rho_c$, an expanding shell is not anticipated to form in the high-density ambient matter.

One of the two solutions of equation (12) increases according to the increase of $L_w$, while the other decreases. Therefore, the former is the only physically plausible solution. This solution is tabulated versus $L_w/\rho_c$ in CGS units in Table 1, where we used $M_{11} = M_G/10^{11}\ M_\odot$ and $r_{10} = r_c/10$ kpc.

### b) *Fragmentation of Dense Shell*

The expanding thin shell can be gravitationally unstable (Ostriker and Cowie 1981; Tomisaka and Ikeuchi 1985). According to the energy principle of Ostriker and Cowie (1981), the instability criterion is that the total energy of a disklike fragment with the radius $d$ cut out of the dense shell is negative:

$$E = (V_s/R_s)^2 d^2/4 - \kappa\pi G\Sigma_g d + 3\Sigma_I/2\Sigma_g < 0,$$

where the geometrical factor $\kappa$ is 0.8449, and

$$\Sigma_g = \int_{\Delta R_s} \rho_s\, dr, \quad \Sigma_I = \int_{\Delta R_s} P_s\, dr.$$

In this criterion, it is required for the gravitational instability of the shell that

$$E_{\min} = \frac{3}{2}\frac{\Sigma_I}{\Sigma_g} - \left(\frac{\kappa\pi G R_s \Sigma_g}{V_s}\right)^2 < 0 \quad (16)$$

at the disk radius $d_m = \kappa G M_s/2V_s^2$. The gravitational instability, with the aid of the Rayleigh-Taylor instability, causes the fragmentation of the shell, and consequently stars are formed on the shell (Fabian, Nulsen, and Stewart 1980; Williams and Christiansen 1985). We tentatively estimate the fragmentation epoch by means of the condition (16) for a typical case where $L_w = 10^{42}$ ergs s$^{-1}$, $M_G = 10^{11}\ M_\odot$, $\rho_c = 10^{-27}$ g

TABLE 1

SIMILARITY SOLUTION

| $L_w/\rho_c$ ($\times 10^{69} r_{10}^{1/2} M_{11}^{3/2}$) | $a$ ($\times 10^{18} M_{11}^{1/2}$) |
|---|---|
| 1 | 2.11 |
| $10^{1/2}$ | 7.42 |
| 10 | 14.6 |
| $10^{3/2}$ | 25.0 |
| $10^2$ | 40.3 |
| $10^{5/2}$ | 62.6 |
| $10^3$ | 95.4 |

© American Astronomical Society • Provided by the NASA Astrophysics Data System

1987ApJ...319..601U



$cm^{-3}$, $r_c = 10$ kpc, and $T_s = 10^4$ K (Williams and Christiansen 1985). As a result, the time when the condition (16) is satisfied for the first time is found to be $t_{\rm frag} = 5.5 \times 10^8$ yr. Then we obtain

$$R_s(t_{\rm frag}) = (at_{\rm frag})^{2/3} = 36 \text{ kpc}\,, \quad V_s(t_{\rm frag}) = 42 \text{ km s}^{-1}\,,$$

and

$$M_s(t_{\rm frag}) = 8\pi\rho_c r_c^{1/2}[(a + l)t_{\rm frag}]^{5/3}/5 = 2.4 \times 10^{10}\ M_\odot\,,$$

where we used the values in Table 1 for $a$. This value of $M_s$ approximately justifies the assumption of neglecting self-gravity with respect to global motion of the shell. The shell radius is comparable to that of inner observed shells. As for the hot bubble, if it is uniform and the temperature maintains the typical value of a hot galactic wind ($\sim 10^7$ K), we can evaluate the X-ray luminosity as

$$L_X = 1.6 \times 10^{39}(T/10^7 \text{ K})^{-0.65}(\dot{M}/1\ M_\odot \text{ yr}^{-1})^2 \text{ ergs s}^{-1}\,,$$

where we used the cooling function by Raymond, Cox, and Smith (1976). This X-ray luminosity, however, is overestimated because the adiabatic cooling inevitably reduces the temperature. Therefore, it seems hard to account for the observed high X-ray luminosities on a pure wind model, just as has been pointed out by Nulsen, Stewart, and Fabian (1984). It may be indeed necessary to confine the hot gas by the gravity of a significant amount of dark matter (Forman, Jones, and Tucker 1985; Mathews and Loewenstein 1986). This is explored numerically in the following sections.

## III. NUMERICAL MODEL

We simulate the sequential stellar shell formation due to successive collisions between a galactic wind and the accreting gas. Such a process is represented by a schematic illustration in Figure 1. First, the galactic wind interacts with the accreting gas, so that a dense thin gaseous shell is produced. After this dense shell fragments because of gravitational instability and stars form there, the wind can blow through this stellar shell. Subsequently, the wind interacts again with the accreting external gas and generates another dense gaseous shell, which results in the second stellar shell through the gravitational instability. This sequence continues until the newly formed gaseous shell is not subject to the gravitational instability. We examine, with a spherically symmetric model, whether such a scenario is successful for the formation of *multiple* stellar shells and hot X-ray corona. The dark matter, the explosive energy release from young stellar components of shells, and the time variation of the wind luminosity are taken into account.

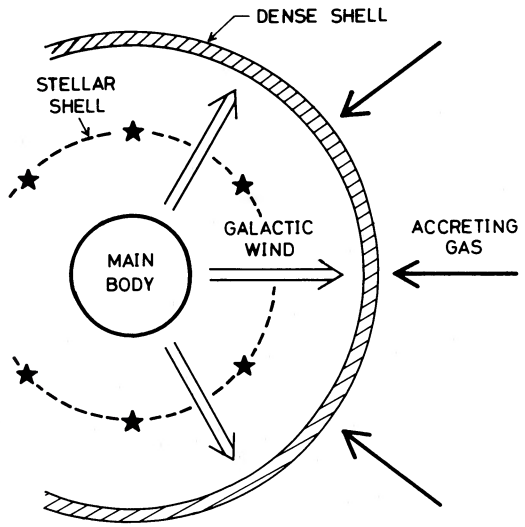


FIG. 1.—Schematic illustration of the sequential stellar shell formation by interactions of a galactic wind with accreting ambient gas.

### a) Galactic Winds and Evolution of Galaxy

In the numerical calculations by Mathews and Baker (1971) and White and Chevalier (1983), the sonic radius arises at $\sim$6–7 kpc. Therefore, we simulate the hot supersonic wind outside of the galaxy radius $r_c = 10$ kpc. We set the mass of baryonic matter within $r_c$ to be $M_G = 10^{11}\ M_\odot$. The adopted temperature of a hot wind is $10^7$ K, and the wind velocity lies between the sound velocity corresponding to $10^7$ K ($\sim$365 km $s^{-1}$) and $\sim$2000 km $s^{-1}$. The mass-loss rate $\dot{M}$ can range from $\sim$0.1 to $\sim 10\ M_\odot$ yr$^{-1}$ (Mathews and Baker 1971; Tinsley 1973; Faber and Gallagher 1976).

We consider also the time variation of the wind activity in some model calculations. One of the adopted models for galaxy evolution is that of the bursts of star formation by Sanders (1981). As a typical case, we examine a wind having $\dot{M} = 10\ M_\odot$ yr$^{-1}$ within duration $10^8$ yr and $\dot{M} = 1\ M_\odot$ yr$^{-1}$ in recurrent time $10^9$ yr. Another model is that by MacDonald and Bailey (1981), where the specific mass-loss rate is estimated as

$$\alpha(t) = \dot{M}/M_G = \alpha_0[(t + t_1)/t_0]^{-\beta},$$

with $\alpha_0 = 3.2 \times 10^{-12}$, $\beta = 1$, $t_0 = 10^{10}$ yr, and $t_1 = 10^7$ yr.

### b) Accreting Gas and Dark Matter

We postulate the power-law initial density distribution for the accreting gas:

$$\rho_{g0}(r) = \rho_c(r/r_c)^{-p}\,.$$

The case of a relatively flat distribution $p = \frac{1}{2}$, which has a similarity solution, and the case of a steep distribution $p = 2$ are compared with each other. The total mass of the accreting gas $M_{gt}$ can be estimated in terms of the galaxy mean number density, $n_G \approx 0.01$ Mpc$^{-3}$, and the baryon mean mass density in units of the critical density, $\Omega_b \approx 0.05$ (Yang *et al.* 1984). The whole mass of baryonic matter which can be assigned to a galaxy is

$$M_b \approx \frac{\rho_{\rm crit}\Omega_b}{n_G}$$

$$\approx 3 \times 10^{11}\left(\frac{n_G}{0.01 \text{ Mpc}^{-3}}\right)^{-1}\left(\frac{\Omega_b}{0.05}\right) M_\odot\,. \qquad (17)$$

Thus, taking $M_G = 10^{11}\ M_\odot$ into account, we adopt

$$M_{\rm gt} \approx M_b - M_G \sim O(10^{11}\ M_\odot)\,.$$

The velocity of accreting gas is presumed to be the infall velocity determined by equations (6) and (7) with

$$M = M_G + M_g(r)\,, \quad M_g(r) = \int_{r_c}^{r} \rho_g\, dr\,, \quad \text{and} \quad \delta(z_{\rm GF}) = 1$$

at $z_{\rm GF} = 3$ (Wyse 1985). In addition, in the further external region as far as $>1$ Mpc, we put a uniform intergalactic gas with the local escape velocity and density of $10^{-29}$ g cm$^{-3}$.

© American Astronomical Society • Provided by the NASA Astrophysics Data System

1987ApJ...319..601U



This density is estimated by

$$\bar{\rho} = \rho_{\rm crit}(1 + z_{\rm GF})^3 \Omega_b \, .$$

The initial temperature of both accreting gas and intergalactic gas is assumed to be $10^4$ K because the almost complete ionization of intergalactic hydrogen has been confirmed by the Gunn-Peterson test (Gunn and Peterson 1965).

For the dark matter, we assume a fixed isothermal distribution specified by the velocity dispersion $\sigma_d$ and the central density $\rho_{d0}$. We adopt here two types of models: one is specified by $\sigma_d = 100$ km s$^{-1}$ and $\rho_{d0} = 10^{-25}$ g cm$^{-3}$ (model A), which includes the mass of $6 \times 10^{11}\ M_\odot$ within 100 kpc, and the other is by $\sigma_d = 200$ km s$^{-1}$ and $\rho_{d0} = 10^{-24}$ g cm$^{-3}$ (model B), which includes the mass of $2 \times 10^{12}\ M_\odot$ within 100 kpc.

### c) *Star Formation and Dynamics of Stellar Shells*

In this numerical analysis, the self-gravity of shells is involved faithfully. For the gravitational instability condition of self-gravitating thin gaseous shells, we use the Ostriker and Cowie criterion which is expressed as equation (16). Besides this condition, in the presence of dark matter, it is also required that the density of a gaseous shell should dominate that of dark matter because the extended dark matter may restrain the gravitational instability (Ikeuchi 1986; Umemura and Ikeuchi 1986). The shell which once satisfies the instability condition is regarded as a collisionless shell composed of stars and dense clouds. The mass fraction of the stellar component in a collisionless shell is chosen to be $f_{\rm star} = 0.1$ (Cohen and Kuhi 1979). If the collisionless shells fall onto $r_c$, then the stellar component is reflected on the surface on $r_c$, and the dense cloud component coalesces into the main body of the galaxy.

### d) *Energy Release from Stellar Shells*

If massive stars are born in stellar shells, they release an explosion energy. For some cases, we include the energy input from stellar shells, assuming $f_{\rm star} = 0.1$ and the Salpeter initial mass function, that is, $\varphi(m) = \varphi_0 m^{-(1+s)}$, with $s = 1.35$ for $0.1 \le m \le 50\ M_\odot$ (Salpeter 1955; MacDonald and Bailey 1981). The lifetime of stars, $\tau$(yr), is calculated in terms of an expression by Larson (1974) as

$$\log \tau = 10.02 - 3.57 \log m + 0.90(\log m)^2 \, ,$$

and the massive stars above 3 $M_\odot$ are made to produce supernova explosions. When such explosive energy release occurs, the dense cloud component in the shell is enforced to disperse, so that the shell consists only of stars, $M_s = M_{\rm star}$. The local energy input rate by a shell is given as $\dot{E} = \epsilon c^2 \dot{M}_s$, where the efficiency $\epsilon$ lies between $10^{-5}$ and $10^{-4}$ (Bookbinder *et al.* 1980).

### e) *Fundamental Equations*

The equations of motion for gas and collisionless systems are expressed in spherical symmetry as

$$\frac{dv_g}{dt} = -\frac{1}{\rho_g}\frac{\partial P_g}{\partial r_g} - \frac{GM_t(r_g)}{r_g^2} \quad \text{for gas} \, , \tag{18}$$

$$\frac{dv_{s,i}}{dt} = -\frac{GM_t(r_{s,i})}{r_{s,i}^2} \quad \text{for } i\text{th shell} \, , \tag{19}$$

where

$$M_t(r) = M_G + 4\pi\left(\int_{r_c}^{r} r^2 \rho_g \, dr + \int_0^r r^2 \rho_d \, dr\right) + \sum_{r_{s,j} < r} M_{s,j} \, . \tag{20}$$

The thermal evolution of gas is governed by

$$\frac{d}{dt} \ln \frac{P_g}{\rho_g^\gamma} = (1 - \gamma)\frac{\Lambda}{P_g} \, , \tag{21}$$

where $\Lambda$ is the cooling rate by Raymond, Cox, and Smith (1976) for $T_g \ge 10^4$ K or that by Dalgarno and McCray (1972) for $T_g < 10^4$ K.

### f) *Numerical Scheme*

In order to simulate the multicomponent system composed of the ambient gas, ejected hot gas, generated collisionless shells, and dark matter, we have developed the spherically symmetric self-gravitating Lagrange scheme of the second order. In this scheme, the mass meshes of gas are created successively to produce a wind. They are annihilated when a stellar shell is born, and then a mass mesh of a collisionless component is created. The number of gas mesh is initially 300. The effectiveness of this scheme has been confirmed by reproduction of the similarity solution for the simplest case.

## IV. NUMERICAL RESULTS

The typical results of model calculations are summarized in Table 2. In this table, $N_{\rm shell}$ is the total number of stellar shells, $R_{s,\,\rm max}$ is the radius of the farthest shell at $10^{10}$ yr, $L_{X,\,\rm max}$ is the maximum X-ray luminosity at 0.5–4.5 keV band during the history of $10^{10}$ yr, and $\Delta\tau_X$ is the duration of X-ray luminosities higher than $10^{39}$ ergs s$^{-1}$. The resultant characteristics of each model are described below.

### a) *Stellar Shells*

In Figure 2, we show the numerical result for model 1 in terms of the density, temperature, velocity, and ionized hydrogen column density versus the radius at $t = 5 \times 10^9$ yr after the outset of the wind activity. The density distribution shows the characteristic structures formed by the interaction of a wind with ambient matter: region 1-, the adiabatically expanding wind ($\rho \propto r^{-2}$, $T \propto r^{-4/3}$) with the constant velocity of $\sim$1000 km s$^{-1}$. This region shows the ionized hydrogen column density as $10^{18}$–$10^{19}$ cm$^{-2}$; region 2-, the inner shock surface; region 3-, the shocked galactic wind where the temperature is raised up to $\sim 10^7$ K due to the thermalization of kinetic energy of the wind; region 4-, the contact discontinuity surface moving at a speed of $\sim$50 km s$^{-1}$; region 5-, the cooled dense shell composed of shocked ambient gas; region 6-, the outer shock surface; region 7-, the accreting gas. By this evolutionary stage, the accreting gas has been almost completely processed into numerous stellar shells, as shown in Figure 3. The mass of the stellar component in each shell ranges from $\sim 10^8$ to $\sim 10^9\ M_\odot$ and the velocities are a few hundred kilometers per second in absolute values. The surface density distribution of stellar shells exhibits sharply edged features. All the shells are built up successively from the inside, and in the outer region, except that some shells have already dynamically evolved and shell crossing has occurred, there are liable to be shells which were formed at the later epoch, as indicated in Figure 3. Such a tendency is also noticeable in the other results (models 2, 5, 8, and 11), as shown in Figure 4. We can see in Figure 4*a* that the stronger the wind is, the fewer the stellar shells are, because the higher velocity of the gaseous shell needs more mass accumulated in the shell for the instability condition (16) to be satisfied. However, the dark matter suppresses the expansion, and therefore a number of stellar

© American Astronomical Society • Provided by the NASA Astrophysics Data System

1987ApJ...319..601U

TABLE 2

TYPICAL RESULTS OF MODEL CALCULATIONS

| Model | $\dot{M}$ ($M_\odot$ yr$^{-1}$) | $V_w$ (km s$^{-1}$) | $p$ | $\rho_c$ (g cm$^{-3}$) | Dark Matter[a] | Energy Release[b] | $N_{shell}$ | $R_{s,max}$ (kpc) | $L_{X,max}$ (ergs s$^{-1}$) | $\Delta\tau_X$ ($10^9$ yr) |
|---|---|---|---|---|---|---|---|---|---|---|
| 1..... | 1 | 1000 | 1/2 | $10^{-27}$ | ... | ... | 11 | 470 | $1 \times 10^{38}$ | 0 |
| 2..... | 10 | $c_s$[c] | 1/2 | $10^{-27}$ | ... | ... | 4 | 330 | $3 \times 10^{38}$ | 0 |
| 3..... | 1 | $c_s$ | 2 | $10^{-26}$ | ... | ... | 21 | 220 | $4 \times 10^{36}$ | 0 |
| 4..... | 1 | $c_s$ | 1/2 | $10^{-28}$ | A | ... | 86 | 190 | $5 \times 10^{39}$ | 8.5 |
| 5..... | 3 | $c_s$ | 1/2 | $3 \times 10^{-28}$ | A | ... | 91 | 250 | $2 \times 10^{40}$ | 4 |
| 6..... | 3 | 1000 | 1/2 | $10^{-28}$ | B | ... | 35 | 280 | $1 \times 10^{40}$ | 8.5 |
| 7..... | 3 | $c_s$ | 1/2 | $10^{-28}$ | B | ... | 5 | 17 | $1 \times 10^{41}$ | >1[d] |
| 8..... | 1 | $c_s$ | 1/2 | $10^{-28}$ | A | $10^{-4}$ | 14 | 180 | $3 \times 10^{39}$ | 1 |
| 9..... | 2 | $c_s$ | 2 | $10^{-26}$ | A | $10^{-4}$ | 14 | 190 | $5 \times 10^{38}$ | 0 |
| 10..... | 1 | 1000 | 2 | $10^{-26}$ | A | $10^{-5}$ | 35 | 210 | $1 \times 10^{39}$ | 2 |
| 11..... | S[e] | $c_s$ | 2 | $10^{-26}$ | A | ... | 96 | 470 | $1 \times 10^{41}$ | 5 |
| 12..... | MB[f] | 1000 | 1/2 | $10^{-27}$ | B | ... | 32 | 310 | $6 \times 10^{40}$ | 4.5 |

[a] Model A has $\rho_{d0} = 10^{-25}$ g cm$^{-3}$ and $\sigma_d = 100$ km s$^{-1}$. Model B has $\rho_{d0} = 10^{-24}$ g cm$^{-3}$ and $\sigma_d = 200$ km s$^{-1}$.

[b] Explosive energy release from young stars in shells with the Salpeter initial mass function is involved for three cases, where the efficiency is specified.

[c] Isothermal sound velocity corresponding to $10^7$ K ($\sim$365 km s$^{-1}$).

[d] No outflow exists. The calculation was terminated at $10^9$ yr.

[e] Time-dependent mass-loss rate of the Sanders type.

[f] Time-dependent mass-loss rate of the MacDonald and Bailey type.

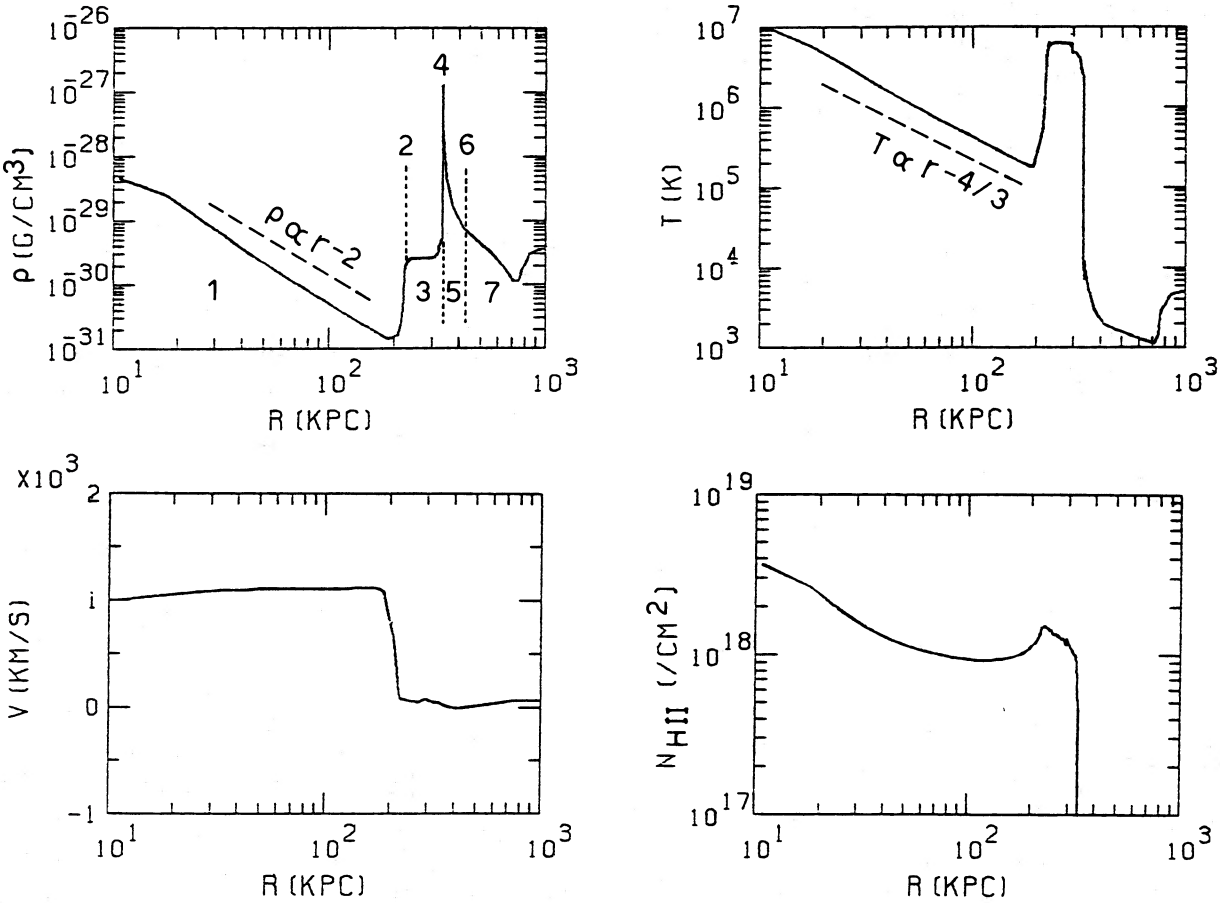


FIG. 2.—Characteristic quantities such as the density $\rho$, temperature $T$, velocity $v$, and ionized hydrogen column density $N_{H II}$ are shown vs. the radius $r$ at $t = 5 \times 10^9$ yr for model 1. The structure is characterized by the several regions as summarized in the text. The adiabatic evolution of $\rho$ and $T$ is also indicated by dash-dotted lines.

© American Astronomical Society • Provided by the NASA Astrophysics Data System

1987ApJ...319..601U



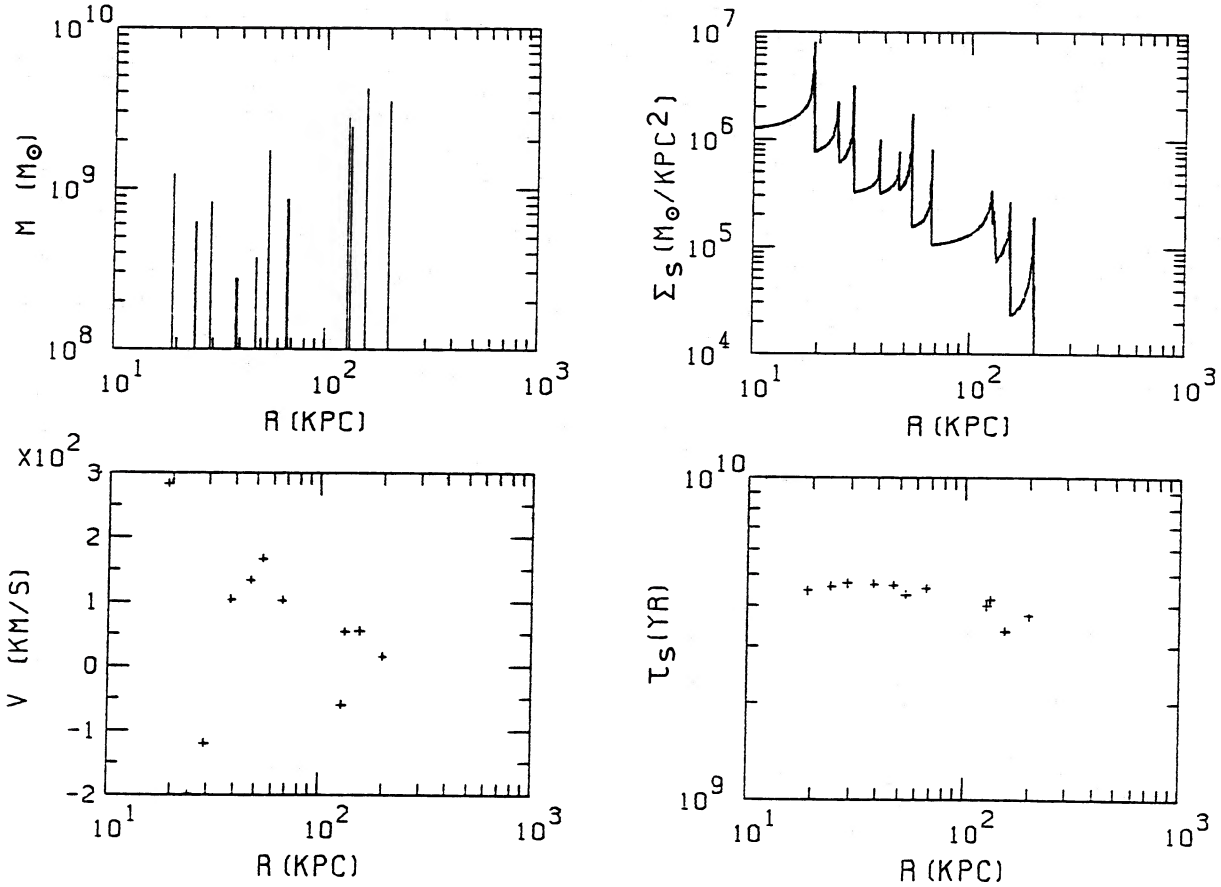


FIG. 3.—Radial distributions of the mass, the surface mass density, the velocity, and the age of the stellar component are shown with respect to stellar shells. The sharply edged features of surface density are clear, and it is noticeable that the shells formed later tend to be located in the outer region.

shells are easily generated (see Fig. 4*b*). The explosive energy release from stellar shells reduces the shell number because the enhanced thermal energy of hot bubble gives rise to a large expansion velocity of the gaseous shell (Fig. 4*c*). However, the periodic activity based on the bursts of star formation does not have much influence on the formation of stellar shells (Fig. 4*d*).

The present calculations show that the formation of the multiple stellar shells extended as far as a few of 100 kpc is a natural consequence of the successive interactions of a galactic wind with the accreting ambient matter. The observability of such stellar shells and the effect of velocity dispersion of stars in shells are discussed in § V.

### *b) X-Ray Coronae*

In the absence of dark matter, X-ray luminosities are generally far below the detection limit of $\sim 10^{39}$ ergs s$^{-1}$ (Mathews and Baker 1972; MacDonald and Bailey 1981; White and Chevalier 1983; Nulsen, Stewart, and Fabian 1984). This is the case also in our numerical calculations (e.g. models 1, 2, and 3). As seen in Figure 2, the ram pressure of accreting matter is by itself insufficient to confine the hot gas without dark matter. We present a result in the case with dark matter in Figure 5, where we show the radial distributions of gas density, temperature, velocity, and X-ray emission rate at the 0.5–4.5 keV band integrated along a line of sight,

$$\Sigma_X = \int \Lambda ds \, .$$

It is found that when the dark matter dominates, the hot galactic wind is decelerated efficiently by the gravity of dark matter, so that the temperature of the hot corona does not cool adiabatically. Consequently, the hot corona has a high X-ray luminosity. The X-ray surface density distributions and luminosities for models 5 and 6 are shown in Figure 6. The hot coronae which have the extension of 40–80 kpc and the X-ray luminosities of $10^{39-40}$ ergs s$^{-1}$ are formed by hot galactic winds confined within the dark matter. The X-ray luminosity depends upon the depth of the gravitational potential of dark matter. The deeper the potential of dark matter is, the higher the X-ray luminosity is. The time evolution of X-ray luminosity is plotted in Figure 7 for models 4, 6, 11, and 12. In models 4 and 6, $L_X$ exceeds $10^{39}$ ergs s$^{-1}$ during (8–9) $\times 10^9$ yr and decreases rapidly in a time scale of $10^9$ yr. This fadeout of $L_X$ is due to a rapid outflow of hot gas in the outer envelope. The bursts of star formation (model 11) raise the X-ray luminosity to $\sim 10^{41}$ ergs s$^{-1}$ for a relatively short period ($\sim 3 \times 10^9$ yr). The time-dependent galactic wind model (model 12) by MacDonald and Bailey (1981) attains luminosities as high as $10^{40-41}$ ergs s$^{-1}$ at an early epoch ($\lesssim 4 \times 10^9$ yr).

It turns out that $\sim 10$ times as much dark matter as the main body of the galaxy is required to account for such high X-ray luminosities as universally observed around elliptical galaxies.

### *c) Critical Wind Luminosity*

The galactic wind cannot always flow far outward against the ram pressure of accreting matter. In order to maintain

© American Astronomical Society • Provided by the NASA Astrophysics Data System

1987ApJ...319..601U

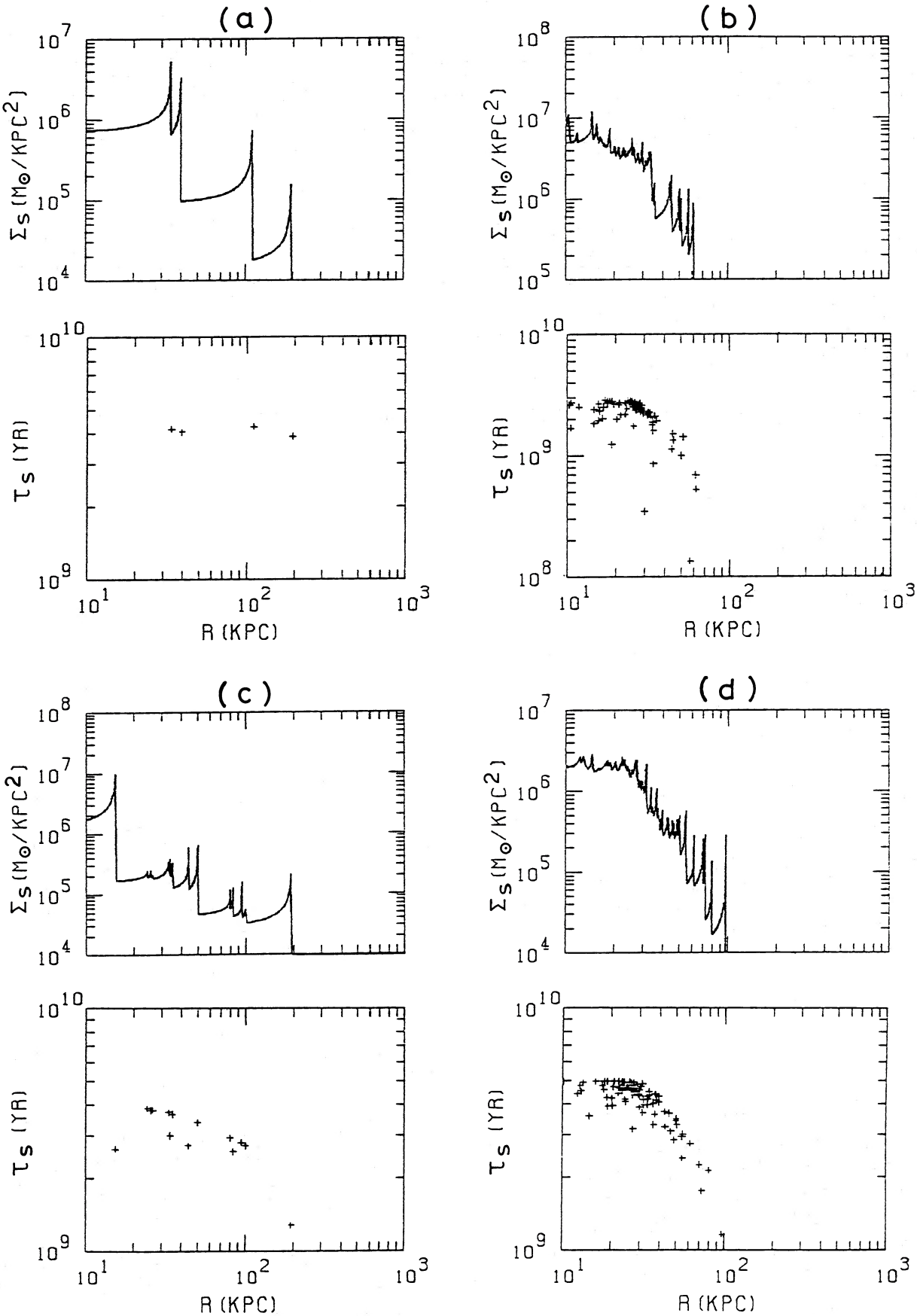


FIG. 4.—Surface density and ages of stellar shells are shown for (*a*) model 2 ($t = 5 \times 10^9$ yr), (*b*) model 5 ($t = 3 \times 10^9$ yr), (*c*) model 8 ($t = 4 \times 10^9$ yr), and (*d*) model 11 ($t = 5 \times 10^9$ yr). Younger shells tend to be located farther from the main body of galaxy. The number of stellar shells decreases with increasing expansion velocity of wind-driven dense shells, and vice versa.

© American Astronomical Society • Provided by the NASA Astrophysics Data System

1987ApJ...319..601U



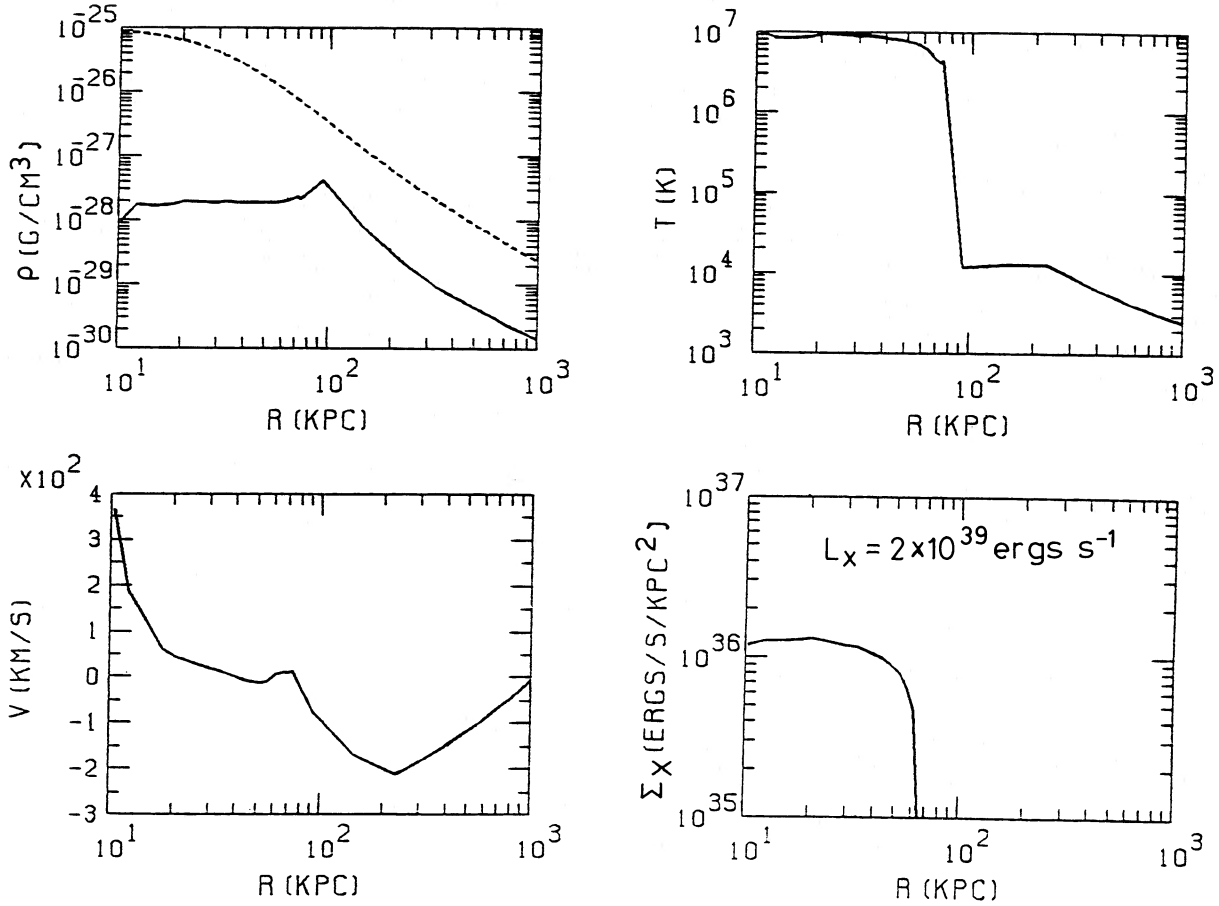


FIG. 5.—Density, temperature, velocity, and X-ray (0.5–4.5 keV) surface density distributions at $5 \times 10^9$ yr for model 4 are shown. Dark matter density distribution is indicated by a dotted line. Total X-ray luminosity at 0.5–4.5 keV band is $2 \times 10^{39}$ ergs $s^{-1}$.

outflow, the wind luminosity must exceed a certain critical value, $L_{w,\,\mathrm{crit}}$. We have found in the similarity analysis that in a point source model for the galactic wind, the wind cannot give rise to an outflow unless it satisfies condition (14). The critical wind luminosities are obtained for more realistic situations by means of numerical calculations. In Figures 8*a* and 8*b*, the critical luminosities are plotted in terms of the initial density of accreting gas at $r_c = 10$ kpc, for the cases of $p = \frac{1}{2}$ and $p = 2$, respectively. Heavy solid lines represent the critical luminosity $L_{w,\,\mathrm{crit}}$ provided by standard model calculations, where no dark matter and no explosion energy are included. In the presence of dark matter model A, $L_{w,\,\mathrm{crit}}$ is shown by heavy dash-dotted lines. It is found that a significant amount of dark matter raises $L_{w,\,\mathrm{crit}}$ because the ram pressure of the accretion flow increases owing to the enhancement of infall velocity by the dark matter. As shown in Figure 9, if the wind luminosity is less than the critical luminosity, no extended stellar shell system is built up, while the hot X-ray corona can be formed.

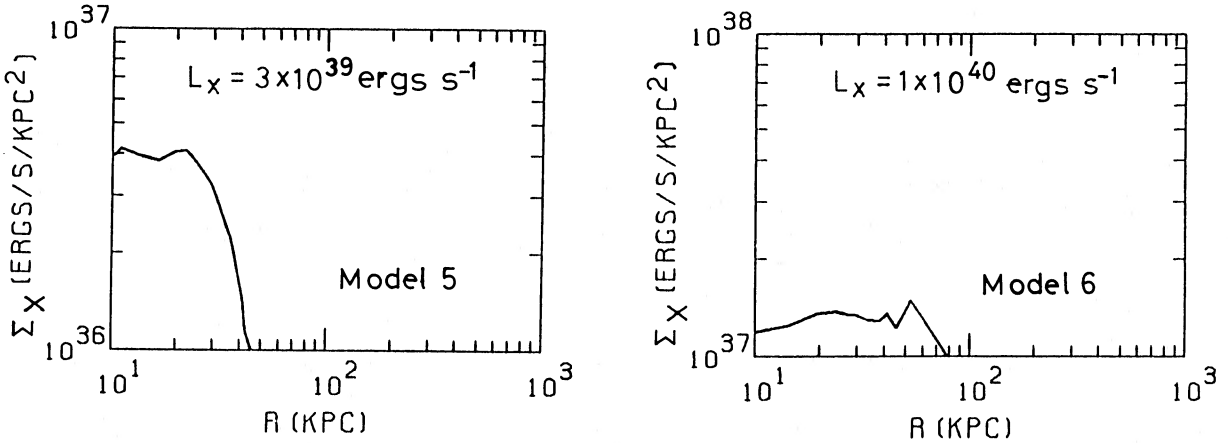


FIG. 6.—The X-ray surface density distributions and total luminosities at 0.5–4.5 keV band, at $3 \times 10^9$ yr for models 5 and 6

© American Astronomical Society • Provided by the NASA Astrophysics Data System

1987ApJ...319..601U



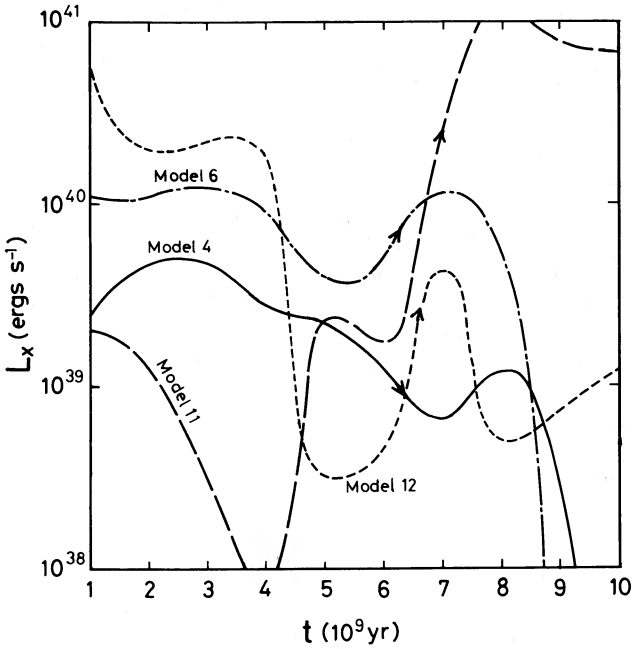


FIG. 7.—Time evolution of X-ray luminosity for models 4, 6, 11, and 12

So X-ray coronae with high luminosities are generally expected, if there is dark matter. The quantity $L_{w,\,\mathrm{crit}}$ in the case with explosive energy release from the shells within the dark matter of model A is shown by dashed lines in Figures 8*a* and 8*b*, where the efficiency is assumed to be $\epsilon = 10^{-4}$. The explosive energy release energizes the hot wind, so that $L_{w,\,\mathrm{crit}}$ is reduced appreciably.

On the other hand, another condition for the successful formation of stellar shells is imposed because the excessively strong wind gives rise to so large an expansion velocity of dense shell that the shell cannot fragment by gravitational instability, bearing no stars there. In Figures 8*a* and 8*b*, we also show another characteristic luminosity, $L_{w,\,b}$, above which the instability condition (16) is never satisfied. Light solid lines represent $L_{w,\,b}$ for the case without dark matter, and light dash-dotted lines represent $L_{w,\,b}$ in the dark matter of model A. In the result, the wind luminosity should lie between $L_{w,\,\mathrm{crit}}$ and $L_{w,\,b}$ for the successful formation of extended stellar shells.

By the comparison of Figure 8*a* with Figure 8*b*, we see that for the relatively flat ($p = \frac{1}{2}$) density distribution of accreting gas, both $L_{w,\,\mathrm{crit}}$ and $L_{w,\,b}$ are significantly larger than those in the steep density distribution of $p = 2$.

## V. DISCUSSION

### *a) Comparison with Observations on Shell Properties*

#### i) *Surface Brightness and Stellar Velocity Dispersion*

Malin and Carter (1980) estimated a lower limit for the surface brightness of the outermost ($\sim 180$ kpc) shell of NGC 3923 to be 30 mag arcsec$^{-2}$. Malin and Carter (1983) reported that the brightest part of the shell around NGC 1344 has a surface brightness of 26.5 mag arcsec$^{-2}$. These surface brightness $S$ can be converted to the surface mass density $\Sigma_s$:

$$\Sigma_s = 3.3 \times 10^4 \left(\frac{M}{L}\right)_{\mathrm{star}} M_\odot \ \mathrm{kpc}^{-2} \quad \text{for } S = 30 \text{ mag arcsec}^{-2}, \quad (22)$$

and

$$\Sigma_s = 8.3 \times 10^5 \left(\frac{M}{L}\right)_{\mathrm{star}} M_\odot \ \mathrm{kpc}^{-2} \quad \text{for } S = 26.5 \text{ mag arcsec}^{-2}. \quad (23)$$

Since the mass-to-luminosity ratio for a stellar component, $(M/L)_{\mathrm{star}}$, can be inferred to be $\sim 1$–3 (Faber and Gallagher 1979), we can expect to detect the shells having

$$\Sigma_s \gtrsim 3 \times 10^4 \ M_\odot \ \mathrm{kpc}^{-2}.$$

Hence, almost all the stellar shells shown in Figure 4 are observable. The stellar shells are characterized by sharply edged features (Malin and Carter 1983; Quinn 1984). Such features are common in the present results (Fig. 4).

The mass of the most unstable fragment in the dense shell (Ikeuchi and Umemura 1984) is estimated to be $10^{4-6}\ M_\odot$, and therefore the stars are expected to be born as clusters. If these star clusters have velocity dispersion, the sharply edged multiple stellar shells are dispersed. In Figure 10, we present the surface density distributions for model 2 ($t = 5 \times 10^9$ yr) and model 8 ($t = 4 \times 10^9$ yr) in the case where the shells are assumed to disperse with time as

$$\Delta R_s = \sigma_s (t - t_f),$$

$t_f$ being the epoch of stellar shell formation. We chose the velocity dispersion to be $\sigma_s = 10$ km s$^{-1}$. We can infer from Figure 10 the time scale when numerous stellar shells exhibit sharply edged features:

$$\Delta\tau_{\mathrm{shell}} \approx 5 \times 10^9 \left(\frac{\sigma_s}{10 \text{ km s}^{-1}}\right)^{-1} \text{yr}. \quad (24)$$

Thus, if all the multiple shells have the age of $\sim 10^{10}$ yr, the stellar velocity dispersion in the shells must be less than several kilometers per second. However, the estimation (24) is based on a too simple argument. The dynamical evolution of stars born in shells needs to be pursued more properly by $N$-body simulations (Umemura 1987).

In addition, Pence (1986) and Fort *et al.* (1986) have observed that the photometric profiles of shells are not so peaked. The peaked features presented in Figure 4 may be blunted by a dispersive stellar distribution in a shell.

#### ii) *Shell Distribution and Total Mass*

On the distribution of stellar shells, it has been pointed out for the clean shell galaxies such as NGC 1344 or NGC 3923 that the spacing between adjacent shells tends to increase with their distance from the galactic center (Quinn 1984; Dupraz and Combes 1986; Hernquist and Quinn 1987). In the present scenario, the distribution of shells is variable with the lapse of time, so the regular spacing should be interpreted as a coincidental result. In Figure 11, the distribution of shells at $t = 10^{10}$ yr of model 9 is compared with that seen in the northeast of NGC 3923 and both are in coincidence. In this figure, the estimated lower limit (22) of $\Sigma_s$ for detectability is also indicated.

Fort *et al.* (1986), based on measurement of the CCD surface photometry of shells, estimated the apparent thickness of the relatively inner shells. For instance, it is $\sim 740$ pc for a shell at $\sim 20$ kpc of NGC 3923. Such thickness is also characteristic in Figure 11.

On the other hand, Fort *et al.* (1986) estimated the total mass

© American Astronomical Society • Provided by the NASA Astrophysics Data System

1987ApJ...319..601U

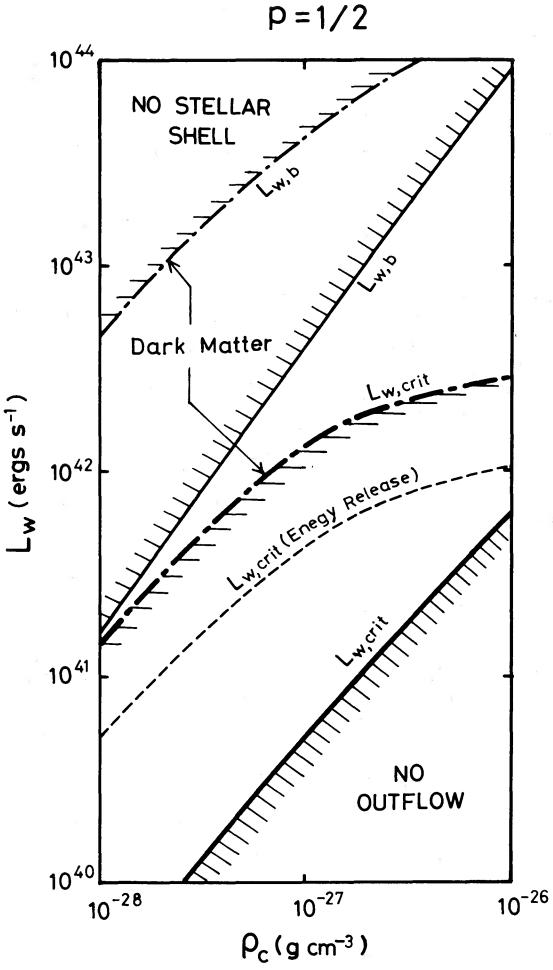


FIG. 8*a*

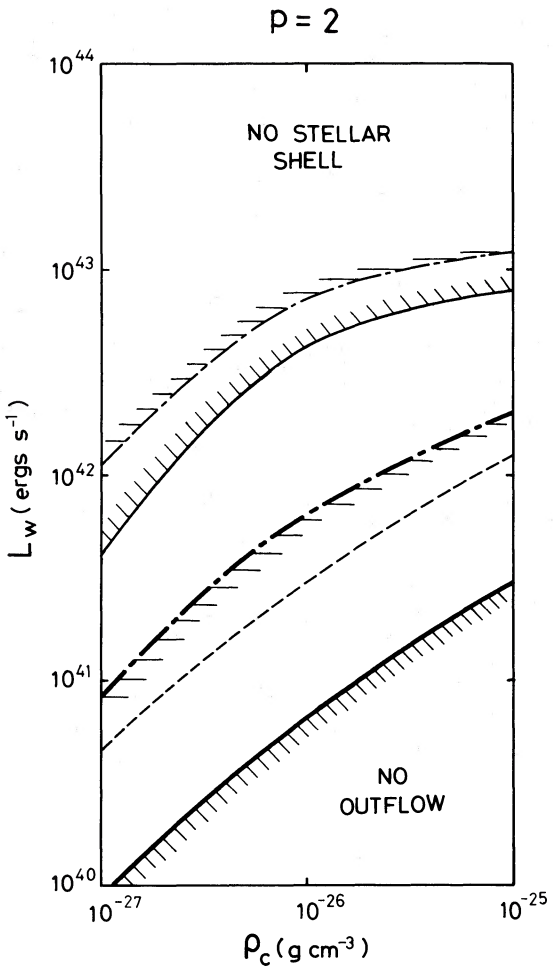


FIG. 8*b*

FIG. 8.—(*a*) Critical luminosities for the formation of the extended stellar shells in the case of $p = \frac{1}{2}$. Heavy solid line and heavy dash-dotted line represent the critical luminosities $L_{w,\,crit}$ for the cases without and with the dark matter of model A, respectively. In the case of explosive energy input from stellar shells with the efficiency $\epsilon = 10^{-4}$, $L_{w,\,crit}$ is shown by a dashed line; $L_{w,\,b}$, above which no stars are born in the shell, is shown by light solid line and light dash-dotted line, respectively, for the cases without and with the dark matter of model A. (*b*) Same as (*a*), but for $p = 2$; $L_{w,\,crit}$ and $L_{w,\,b}$ are considerably smaller than those for $p = \frac{1}{2}$.

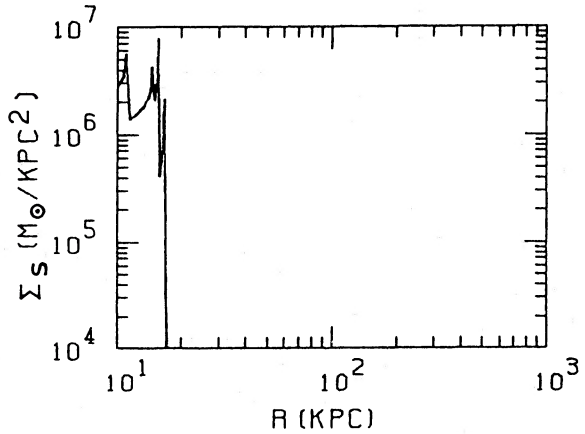


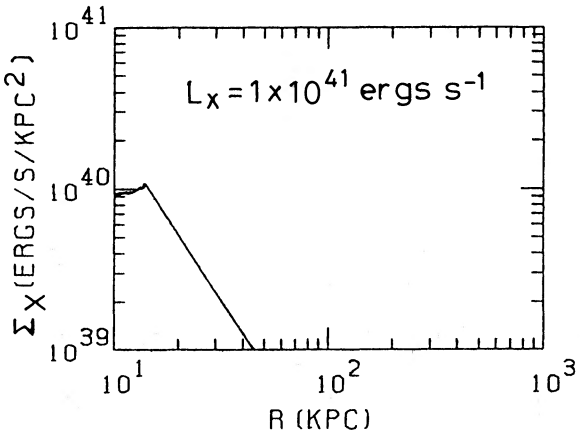


FIG. 9.—Stellar shells and X-ray corona in the case of $L_w < L_{w,\,crit}$ at $10^9$ yr on model 7. No extended stellar shells are created, but the hot corona with the high X-ray luminosity can be formed.

© American Astronomical Society • Provided by the NASA Astrophysics Data System

1987ApJ...319..601U



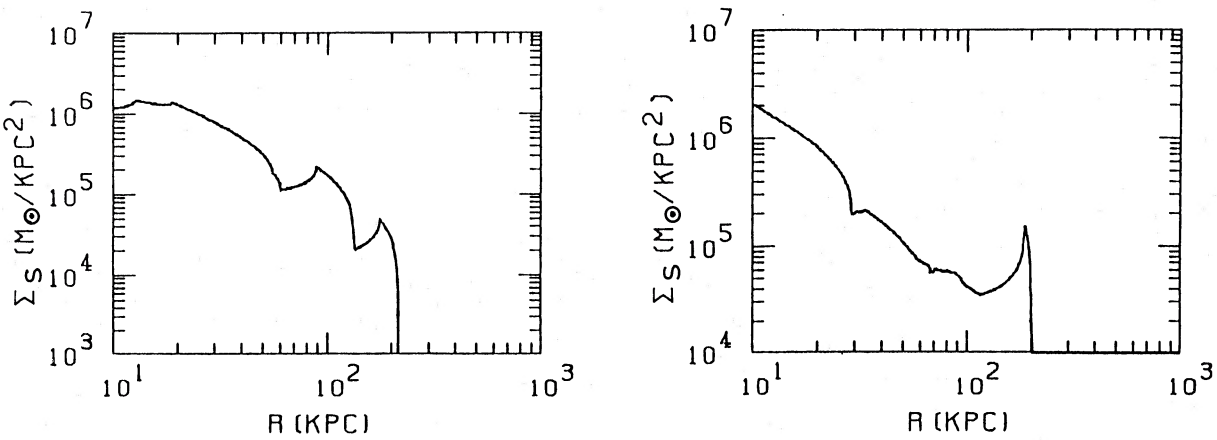


FIG. 10.—Surface mass density distributions of the stellar shells broadened by the stellar velocity dispersion of 10 km s$^{-1}$ for model 2 ($t = 5 \times 10^9$ yr) and model 8 ($t = 4 \times 10^9$ yr) are shown, which should be compared with those in Fig. 4.

of shell systems to be $\sim 10\%$ of the galaxy mass, and, in particular, for NGC 3923 it is between 3% and 8%. This well agrees with the total mass fraction $\sim 5\%$ of such a shell system as shown in Figure 11. (It is noted that Pence 1986 inferred much smaller fraction for comparatively inner shells around NGC 3923.)

Here we note that the stellar shells generally exhibit incomplete circles, which tend to be aligned with the major axis and seem to be interleaved in radii around the underlying galaxy showing an apparent eccentricity (>E3). Such regularity is a fundamental characteristic of the shell system, which has been well simulated in merger hypothesis. In addition, the distribution of shells at radii less than 10 kpc may give an important constraint on which theory is appropriate (Quinn 1984; Dupraz and Combes 1986; Fort *et al.* 1986; Hernquist and Quinn 1987). For the investigation of these points, the dynamical evolution of stellar shells under a nonspherical potential should be pursued by three-dimensional $N$-body calculations (Umemura 1987).

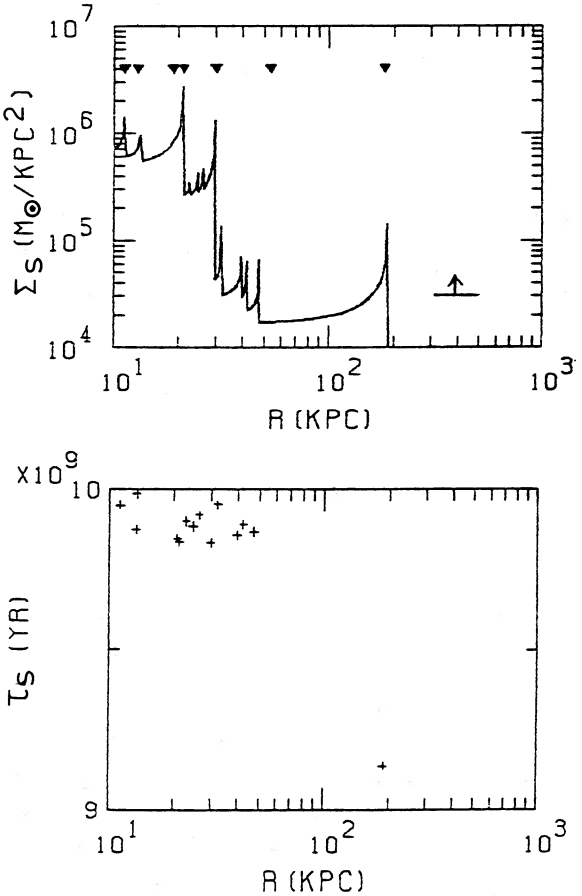


FIG. 11.—Distribution of stellar shells in model 9 ($t = 10^{10}$ yr) is compared with that of shells observed in the northeast of NGC 3923 (*filled triangles*). Lower limit of $\Sigma_s$ for detectability is indicated by a barred arrow. The ages of stellar shells are plotted in the linear scale with respect to the vertical axis.

iii) *Color Indices*

The colors of the shells around NGC 1344 are consistent with the disk population of stars rather than an elliptical population, although not so blue as expected for the recently formed stars (Carter, Allen, and Malin 1982). Fort *et al.* (1986) have shown that shells around NGC 2865 and NGC 5018 are distinctly bluer than the main body, whereas the shells around NGC 3923 have an approximately similar color to that of the main body. Recently, Pence (1986) showed that the shells around NGC 3051 and NGC 3923 appear to consist of a similar stellar population to the main body.

In the present scenario, the stellar shells are not older than the main body of the galaxy. The apparently bluer shells can be interpreted as shells formed by the relatively recent wind activity, while the shells having nearly the same color as the main body, such as shells around NGC 3923, can be considered as shells formed by the early activity of the galaxy. Moreover, the younger stellar shells tend to be located in the outer region, as remarked in §IV*a*. This tendency can be tested by the comparison among the color indices of the inner and the outer shells in a wide range of radii.

*b) Comparison with Observations on X-Ray Coronae*

Forman, Jones, and Tucker (1985) fitted the X-ray surface brightness distributions to the form as

$$S(r) = S(0)[1 + (r/h)^2]^x ,$$

for 13 early-type galaxies having high X-ray luminosities, and found that $x$ ranges from $-2.5$ to $-0.7$ and $h$ ranges from 2 kpc to 10 kpc. The distributions shown in Figure 6 may not be in precise agreement with the observed ones. It is because

© American Astronomical Society • Provided by the NASA Astrophysics Data System

1987ApJ...319..601U



the galaxy has been approximated as a hard sphere of 10 kpc, for convenience on the numerical technique. In order to examine the distribution of hot gas in more detail, one needs to employ a model of mass distributions of elliptical galaxies (Mathews and Loewenstein 1986). It, however, is emphasized here that the total amounts of hot gas accumulated in the envelopes of galaxies are expected not to be largely affected by this simplification because they substantially depend on the depth of potential. The present numerical calculations show that the X-ray luminosities are, without dark matter, far below those observed. In the presence of dark matter, according to increase of its amount, more hot gas is confined in the envelope of the galaxy. So the hot corona can emit as large an amount of X-ray as observed. In order for $10^{39-41}$ ergs $s^{-1}$ to be emitted in X-ray, nearly 10 times as much dark matter as the baryonic matter is required for the galaxy.

### c) *Environmental Effects*

As an important statistical property, shell galaxies are preferentially found in the regions of low galaxy density (Malin and Carter 1983; Schweizer and Ford 1985). If we adopt $T_w = 10^7$ K, $V_w = 1000$ km $s^{-1}$, and $\dot{M} = 1\ M_\odot\ yr^{-1}$ as typical wind parameters, the wind luminosity becomes $L_w = 4.4 \times 10^{41}$ ergs $s^{-1}$ from equation (15). The conditions for the successful formation of extended stellar shells are imposed by $L_{w,b}$ and $L_{w,\mathrm{crit}}$ in Figures 8*a* and 8*b*. Here we use the characteristic luminosities in the presence of dark matter because dark matter is necessary for the high X-ray luminosity. The condition by $L_{w,b}$ is roughly satisfied if the accreting gas density is several times as large as the mean baryon density of the universe at $z_{GF}$ ($\sim 10^{-29}$ g $cm^{-3}$). Such density is naturally expected in a galaxy formation process from density fluctuations. The condition by $L_{w,\mathrm{crit}}$ is given as $\rho_c \lesssim 3 \times 10^{-28}$ g $cm^{-3}$ for $p = \frac{1}{2}$ and $\rho_c \lesssim 5 \times 10^{-27}$ g $cm^{-3}$ for $p = 2$. If the explosion energy is released from stellar shells, the condition is replaced by $\rho_c \lesssim 1 \times 10^{-27}$ g $cm^{-3}$ for $p = \frac{1}{2}$ and $\rho_c \lesssim 2 \times 10^{-26}$ g $cm^{-3}$ for $p = 2$. Under the reasonable assumption that the accreting gas density is higher in the cluster regions than in the vicinity of isolated galaxies, this condition can be interpreted such that the extended shell structures can hardly form around galaxies in clusters. This may be a reason why the shell galaxies are preferentially found in the regions of low galaxy density, although we are, of course, left with the possibility of the tidal disruption of shell structures in the regions of high galaxy density. On the other hand, the X-ray coronae with high luminosities can be generally expected in the presence of dark matter, even if the wind luminosities do not exceed the critical ones.

In this paper, we have presented a wind-accretion flow interaction model as a new scenario of the formation of multiple stellar shells as well as hot X-ray coronae and have shown that this scenario is successful in not a few points. In the present spherically symmetric analysis, the general nonspherical regularity of shells and the diversity of shell features have not been examined. These are future problems for this scenario.

We are grateful to Professor S. Sakashita for his precious advice and continuous encouragement. We thank also D. Malin for providing the photographic reproduction of a few shell galaxies; W. Forman for offering the X-ray contour maps of some elliptical galaxies; M. Sasaki for stimulating discussion on shell galaxies; M. Hattori and A. Habe for useful remarks on X-ray coronae; M. Iye, K. Kodaira, S. Okamura, F. Takahara, Y. Uchida, Y. Yoshii, and the colleagues in our school for precious comments. This research was supported in part by the Grants-in-Aid for Encouragement of Young Scientists of the Ministry of Education, Science, and Culture, No. 61790115, and Scientific Research of the Ministry of Education, Science and Culture, No. 60540153. Numerical calculations were performed by FACOM M380 at Tokyo Astronomical Observatory.

This paper is based on a portion of the doctral dissertation by M. Umemura, submitted to Hokkaido University, in partial fulfillment of the requirements for the doctorate.

## REFERENCES

Athanassoula, E., and Bosma, A. 1985, *Ann. Rev. Astr. Ap.*, **23**, 147.
Avedisova, V. S. 1972, *Soviet Astr.*, **15**, 708.
Bookbinder, J., Cowie, L. L., Krolik, J. H., Ostriker, J. P., and Rees, M. 1980, *Ap. J.*, **237**, 647.
Canizares, C. R., Fabbiano, G., and Trinchieri, G. 1987, *Ap. J.*, **312**, 503.
Carter, D., Allen, D. A., and Malin, D. F. 1982, *Nature*, **295**, 126.
Cohen, M., and Kuhi, L. V. 1979, *Ap. J. Suppl.*, **41**, 743.
Dalgarno, A., and McCray, R. A. 1972, *Ann. Rev. Astr. Ap.*, **10**, 375.
Dopita, M. A. 1981, *Ap. J.*, **246**, 65.
Dupraz, C., and Combes, F. 1986, *Astr. Ap.*, **166**, 53.
Dyson, J. E., and deVries, J. 1972, *Astr. Ap.*, **20**, 223.
Faber, S. M., and Gallagher, J. S. 1976, *Ap. J.*, **204**, 365.
———. 1979, *Ann. Rev. Astr. Ap.*, **17**, 135.
Fabian, A. C., Nulsen, P. E. J., and Stewart, G. C. 1980, *Nature*, **287**, 613.
Forman, W., Jones, C., and Tucker, W. 1985, *Ap. J.*, **293**, 102.
Forman, W., Schwarz, J., Jones, C., Liller, W., and Fabian, A. 1979, *Ap. J. (Letters)*, **234**, L27.
Fort, B. P., Prieur, J.-L., Carter, D., Meatheringham, S. J., and Vigroux, L. 1986, *Ap. J.*, **306**, 110.
Gunn, J. E. 1977, *Ap. J.*, **218**, 592.
Gunn, J. E., and Gott, J. R. 1972, *Ap. J.*, **176**, 1.
Gunn, J. E., and Peterson, B. A. 1965, *Ap. J.*, **142**, 1633.
Hernquist, L., and Quinn, P. J. 1987, *Ap. J.*, submitted.
Huang, S., and Stewart, P. 1985, *Astr. Ap.*, **153**, 189.
Ikeuchi, S. 1986, *Ap. Space Sci.*, **118**, 509.
Ikeuchi, S., and Umemura, M. 1984, *Progr. Theor. Phys.*, **72**, 216.
Larson, R. B. 1974, *M.N.R.A.S.*, **166**, 585.
MacDonald, J., and Bailey, M. E. 1981, *M.N.R.A.S.*, **197**, 995.
Malin, D. F., and Carter, D. 1980, *Nature*, **285**, 643.
———. 1983, *Ap. J.*, **274**, 534.
Mathews, W. G., and Baker, J. C. 1971, *Ap. J.*, **170**, 241.
Mathews, W. G., and Loewenstein, M. 1986, *Ap. J. (Letters)*, **306**, L7.
Nulsen, P. E. J., Stewart, G. C., and Fabian, A. C. 1984, *M.N.R.A.S.*, **208**, 185.
Ostriker, J. P., and Cowie, L. L. 1981, *Ap. J. (Letters)*, **243**, L127.
Peebles, P. J. E. 1982, *Ap. J.*, **257**, 438.
Pence, W. D. 1986, *Ap. J.*, **310**, 597.
Quinn, P. J. 1982, Ph.D. thesis, Australian National University, Canberra.
———. 1984, *Ap. J.*, **279**, 596.
Raymond, J. C., Cox, D. P., and Smith, B. W. 1976, *Ap. J.*, **204**, 290.
Sakashita, S., Hanami, H., and Umemura, M. 1984, *Ap. Space Sci.*, **98**, 315.
Salpeter, E. E. 1955, *Ap. J.*, **121**, 161.
Sanders, R. H. 1981, *Ap. J.*, **244**, 820.
Schweizer, F. 1980, *Ap. J.*, **237**, 303.
Schweizer, F., and Ford, W. K., Jr. 1985, in *Lectures Notes in Physics*, Vol. *New Aspects of Galaxy Photometry*, ed. J. L. Nieto (Berlin: Springer-Verlag), p. 145.
Tinsley, B. M. 1973, *Ap. J.*, **186**, 35.
Tomisaka, K., and Ikeuchi, S. 1985, *Pub. Astr. Soc. Japan*, **37**, 461.
Toomre, A., and Toomre, J. 1972, *Ap. J.*, **178**, 623.
Umemura, M. 1987, in preparation.
Umemura, M., and Ikeuchi, S. 1985, *Ap. J.*, **299**, 583.
———. 1986, *Astr. Ap.*, **165**, 1.
Weaver, R., McCray, R., Caster, J., Shapiro, P., and Moore, R. 1977, *Ap. J.*, **218**, 377.
White, R. E., III, and Chevalier, R. A. 1983, *Ap. J.*, **275**, 69.
Williams, R. E., and Christiansen, W. A. 1985, *Ap. J.*, **291**, 80.
Wyse, R. F. G. 1985, *Ap. J.*, **299**, 593.
Yang, J., Turner, M. S., Steigman, G., Schramm, D. N., and Olive, K. A. 1984, *Ap. J.*, **281**, 493.

S. IKEUCHI and M. UMEMURA: Tokyo Astronomical Observatory, University of Tokyo, Mitaka, Tokyo 181, Japan

© American Astronomical Society • Provided by the NASA Astrophysics Data System